第 29 卷第 12 期 无 机 化 学 学 报 Vol.29 No.12
2013 年 12 月 CHINESE JOURNAL OF INORGANIC CHEMISTRY 2615-2622

纳米 Fe_3O_4 及 Ni^{2+}掺杂 Fe_3O_4 的制备、表征及吸附 Pb(Ⅱ)的特性

魏世勇* 杨小洪
(生物资源保护与利用湖北省重点实验室,湖北民族学院化学与环境工程学院,恩施 445000)

摘要: 采用一种改进的共沉淀法制备了纳米磁铁矿(Fe_3O_4)及 Ni^{2+}掺杂磁铁矿($Ni_xFe_{3-x}O_4$, x=0.1, 0.3, 0.6),用 X-射线衍射(XRD)、扫描电镜(SEM)、氮气物理性吸附、酸碱滴定等手段对产物进行了表征,用平衡吸附法研究了 4 种样品对 Pb(Ⅱ)离子的吸附容量及吸附模型。结果表明,Fe_3O_4 和 3 种 $Ni_xFe_{3-x}O_4$ 均为近似球形的单相晶质纳米颗粒;与 Fe_3O_4 比较,$Ni_xFe_{3-x}O_4$ 的颗粒尺寸变小、表面电荷零点和 pH=5.0 时的表面正电荷量降低;样品的孔体积、比表面积和表面分形度以及表面羟基含量都随产物中 Ni^{2+}掺杂量的增加而升高。4 种样品对 Pb(Ⅱ)的等温吸附数据均适合用 Langmuir 模型拟合(R^2=0.9942~0.9858),其相关系数的大小表现为:Fe_3O_4>$Ni_{0.1}Fe_{2.9}O_4$>$Ni_{0.3}Fe_{2.7}O_4$=$Ni_{0.6}Fe_{2.4}O_4$;Freundlich 模型对样品等温吸附 Pb(Ⅱ)的实验数据拟合度较低(R^2=0.981 3~0.947 7),4 种样品的 Freundlich 相关系数的大小关系与 Langmuir 相关系数相反。初始 pH=5.0 时,Fe_3O_4, $Ni_{0.1}Fe_{2.9}O_4$, $Ni_{0.3}Fe_{2.7}O_4$ 和 $Ni_{0.6}Fe_{2.4}O_4$ 对 Pb(Ⅱ)的最大吸附容量分别为 6.02, 6.68, 7.29 和 8.34 mg·g^{-1}。可见,$Ni_xFe_{3-x}O_4$(尤其是 Ni^{2+}掺杂量较高的产物)对水环境中重金属 Pb(Ⅱ)的去除能力明显高于 Fe_3O_4。

关键词: 纳米 Fe_3O_4; Ni^{2+}掺杂; 表面性质; 吸附; 铅(Ⅱ)
中图分类号: O614.81$^+$1; S153.6$^+$1; P578.4$^+$97 **文献标识码**: A **文章编号**: 1001-4861(2013)12-2615-08
DOI: 10.3969/j.issn.1001-4861.2013.00.377

Preparation, Characterization and Adsorption Characteristics for Pb(Ⅱ) of Fe_3O_4 and Ni-Doped Fe_3O_4 Nanoparticles

WEI Shi-Yong* YANG Xiao-Hong
(*Key Laboratory of Biologic Resources Protection and Utilization of Hubei Province. Department of Chemistry and Environmental Engineering, Hubei University for Nationalities, Enshi, Hubei* 445000, *China*)

Abstract: Nanocrystalline magnetite (Fe_3O_4) and Ni-doped magnetites ($Ni_xFe_{3-x}O_4$, x=0.1, 0.3, and 0.6) were prepared by a modified coprecipitation procedure, and their surface properties and application for the removal of Pb(Ⅱ) ions from aqueous solutions were characterized using X-ray diffraction (XRD), scanning electron microscopy (SEM), nitrogen physical adsorption, potentiometric titrations and batch adsorption experiments. Results show that all the samples are single-phase crystalline nanoparticles with an approximately spherical shape. Compared to Fe_3O_4, the particle size, the pHpzc value and the surface charge at pH=5.0 for $Ni_xFe_{3-x}O_4$ nanoparticles are decreased; and the pore volume, specific surface area (SSA), surface fractal dimension and the content of surface hydroxyls are increased. Langmuir correlation coefficients for Pb(II) adsorption on the samples are fairly high (R^2= 0.9942~0.9858) and they follow the order: Fe_3O_4>$Ni_{0.1}Fe_{2.9}O_4$>$Ni_{0.3}Fe_{2.7}O_4$=$Ni_{0.6}Fe_{2.4}O_4$, and those of Freundlich model are relatively low (R^2=0.9813~0.9477) and the order is opposite to Langmuirs. At pH=5.0, Langmuir adsorption capacities (q_{max}) of Fe_3O_4, $Ni_{0.1}Fe_{2.9}O_4$, $Ni_{0.3}Fe_{2.7}O_4$ and $Ni_{0.6}Fe_{2.4}O_4$ are 6.02, 6.68, 7.29, and 8.34 mg·g^{-1}, respectively. Compared to Fe_3O_4, $Ni_xFe_{3-x}O_4$ nanoparticles with a high content of Ni have a higher adsorption capacity for the Pb(Ⅱ) ions in aqueous solutions.

Key words: magnetite nanoparticles; Ni-doped magnetite; surface properties; adsorption; lead(Ⅱ)

收稿日期:2013-04-08。收修改稿日期:2013-07-19。
国家自然科学基金(No.41261060)和湖北省教育厅科学技术研究计划(No.Q20122904)资助项目。
*通讯联系人。E-mail:xiangju12345@126.com

0 Introduction

Heavy-metal pollution of soils and waters occurs globally. Of the heavy metals, Pb(Ⅱ) is considered a widespread contaminant [1-2]. Accumulation of Pb(Ⅱ) in nature is a serious problem because of its potential transfer through food chain to animals and humans. Some diseases, such as the brain damage, reproductive failures, decrease of the intelligence quotients (IQ), etc., may be caused when Pb(Ⅱ) is excessively taken into the bodies of animals and humans [1,3-4]. Therefore, it is very necessary to remove toxic Pb(Ⅱ) from soils and waters.

Adsorption is a successful method for the removal of heavy metals from soil solutions and aquatic systems. Many researches have focused on the development of novel absorbents with an enhanced adsorption rate and capacity for pollutants [3,4-5]. Magnetite (Fe_3O_4), easily obtained by artificial preparation with cheap and environmentally friendly iron salts, has a high reactivity due to its nano-scale size, a high SSA and large amounts of surface functional groups[5-6]. Therefore, Fe_3O_4 has been widely used as an absorbent for the removal of heavy metals from aqueous solutions[3,5-7].

The doping of metal cations could significantly affect the physical and chemical properties of Fe_3O_4 [8-11]. Increasing attention has been paid to Ni-doped Fe_3O_4 nanoparticles due to their novel properties and potential application as those of permanent magnets, microwave absorbers, catalysts and chemical sensors[8-10,12]. The partial incorporation of Fe^{2+} by Ni^{2+} into Fe_3O_4 crystal structure leads to a significant amelioration in the catalytic activities for the catalytic reactions of N_2O and CO [12-14]. The coercivity, saturation magnetization, conductivity and magnetoresistance of Ni-doped Fe_3O_4 decrease when compared to those of Fe_3O_4 [10,13,15]. Thermogravimetry and differential scanning calorimetry (TG-DSC) analyses show that the substitution of Fe^{2+} by Ni^{2+} stabilizes the Fe_3O_4 structure and enhances its industrial applications [8-9]. The crystal micromorphologies, crystallite sizes, specific surface area, surface charge and surface chemical characteristics of Ni-doped Fe_3O_4 nanoparticles depend on the content of Ni, preparative methods and reaction conditions[8,11-13,15-16].

The magnetic properties, catalytic behaviors, thermal stability and biomedical applications of Ni-doped Fe_3O_4 nanoparticles have been extensively studied [8-10,12-14], and the surface properties were also reported in a few literatures [11,16], but the investigation on its application for the removal of heavy metals from aqueous solutions was very limited. In this study, Fe_3O_4 and Ni-doped Fe_3O_4 nanoparticles were prepared by a modified coprecipitation method. The effects of the Ni^{2+} doping on the crystal structure, morphology, surface properties of Fe_3O_4 were analyzed using X-ray diffractometry (XRD), scanning electron microscopy (SEM), nitrogen physical adsorption, and potentiometric titrations. Moreover, the adsorption characteristics for Pb(Ⅱ) ions by Fe_3O_4 and Ni-doped Fe_3O_4 nanoparticles were further investigated using batch adsorption experiments.

1 Experimental

1.1 Sample preparation

Nanocrystalline Fe_3O_4 was prepared by a modified coprecipitation procedure described in [6]. Briefly, 6.1 g of $FeCl_3 \cdot 6H_2O$ and 4.2 g of $FeSO_4 \cdot 7H_2O$ were dissolved in 100 mL double distilled water (DDW) and heated to 90 ℃. Under N_2 protection and vigorously stirring, a solution of 25% ammonium hydroxide was added until the pH value to 9 ~10. Then 5 mL of 3 $mol \cdot L^{-1}$ oleic acid solution was added to the suspension as a surfactant and coating material. The suspension was brought to 90 ℃ in a glycerin bath and constantly stirred for 2 h. The product was cooled to room temperature, washed five times with DDW and two times with ethanol, and then centrifuged for 20 min at 8 000 $r \cdot min^{-1}$. The precipitate was dried at 90 ℃, ground to pass a 100-mesh sieve, and stored in a desiccator. For the preparation of Ni-doped Fe_3O_4 nanoparticles, a certain amount of $FeSO_4$ was substituted by an equal molar amount of $NiCl_2$ and the total molar amount of Fe(Ⅱ)

and Ni(Ⅱ) in the solution for preparation of Ni-doped Fe_3O_4 was equal to the molar amount of Fe(Ⅱ) in the solution for preparation of Fe_3O_4. The other procedure for preparation of Ni-doped Fe_3O_4 nanoparticles was similar to that of Fe_3O_4. Based on the initial molar ratios of Ni/Fe, the Ni-doped Fe_3O_4 was denoted as $Ni_{0.1}Fe_{2.9}O_4$, $Ni_{0.3}Fe_{2.7}O_4$, and $Ni_{0.6}Fe_{2.4}O_4$, respectively.

1.2 Sample analysis

The content of Ni in Ni-doped Fe_3O_4 was determined as follows. 20 mg sample was dissolved in a 5 mL of 6 mol·L^{-1} HCl solution, oscillated for 8 h, and then centrifuged. The concentration of Ni in the supernatant was measured by a Varian Vista-MPX ICP-OES (ICP). Powder X-ray diffraction (XRD) patterns were measured on a German Bruker D8 ADVANCE X-ray diffractometer. The diffractometer was operated at 40 kV tube voltage and 40 mA tube current with a graphite monochromator using Cu $K\alpha$ radiation (λ=0.154 06 nm), scaning rate of 2°·min^{-1}, and step intervals of 0.02°. Morphology of the samples was analyzed using a field emission scanning electron microscope (FE-SEM; JEOL JSM-6700F).

Surface structural properties of the samples were measured by Quanta Chrome Autosorb-1S apparatus using N_2 as adsorbate. 0.20 g powder sample was degassed for 12 h at 90 ℃ prior to the adsorption measurement. The total pore volume was estimated from the maximum adsorption capacity at relative pressure close to the saturation pressure. The SSA and surface fractal dimension of the samples were calculated from the N_2 adsorption isotherms according to Brunauer-Emmett-Teller (BET) and Barrett-Joyner-Halenda (BJH) method, respectively.

Surface charge properties of the samples were measured by potentiometric titrations using an automatic potentiometric titrator (Metrohm titrator 836). To a titration cell 0.10 g sample and 50 mL of 20 mmol·L^{-1} KCl solution were added. After introduction of electrodes, burette tips, and the N_2 source, the titration cell was closed. Under N_2 refluxing and mechanical stirring, potentiometric titrations were conducted with 0.1 mol·L^{-1} HCl and KOH solutions. The suspension was adjusted to pH value of 3.0 and equilibrated for 30 min, and then the titrations were carried out from pH value of 3.0 to 10.0 using a 0.1 mol·L^{-1} KOH solution. After an additional equilibration time of 30 min, the suspension was titrated back to pH=3.0 using a 0.1 mol·L^{-1} HCl solution. For the next titration round, the ionic strength of the suspension was sequentially increased to two higher levels (80 and 200 mmol·L^{-1} KCl) by adding KCl reagent. After salt addition, the cell was equilibrated for 30 min before continuation of the retitration. For the three KCl concentrations a blank titration was also performed. The titration data from pH value of 10.0 to 3.0 were used to analyze the surface proton charge (q_H) of the samples.

1.3 Adsorption experiments

8 g·L^{-1} stock suspension of adsorbent was prepared by the following procedure. 4 g powder sample and 400 mL DDW were added into a 500 mL polyethylene flask, followed by ultrasonic dispersion for 30 min, and then the volume of the suspension was adjusted to 500 mL with DDW. A 300 mg·L^{-1} Pb(Ⅱ) stock solution was prepared by dissolving $Pb(NO_3)_2$ in DDW.

Batch adsorption experiments were conducted with a 2 g·L^{-1} adsorbent concentration, 20 mmol·L^{-1} KCl background electrolyte, a set of initial Pb(Ⅱ) concentrations (0~150 mg·L^{-1}) and a temperature of 25 ℃. 5 mL stock suspension of adsorbent and 0~10 mL of Pb(Ⅱ) stock solution were taken into a 50 mL stoppered conical flask, followed by adding 2 mL of 200 mmol·L^{-1} KCl to maintain ionic strength. The pH value of the suspension was adjusted to 5.0, and then the volume was adjusted to 20 mL with DDW. The suspension was mechanically agitated for 24 h at a speed of 300 r·min^{-1}, and then filtered through a 0.45 μm Millipore membrane filter. The concentration of the residual Pb(Ⅱ) in the filtrate was determined with atomic absorption spectroscopy (AAS). All experiments were performed in triplicate, and the average values were reported in present study. The adsorption amount for Pb(Ⅱ) by the adsorbent was calculated from the following equation:

$$q_e = (c_i - c_e)/c_a \quad (1)$$

Where q_e is the adsorbed amount ($mg \cdot g^{-1}$); c_i and c_e is the initial and residual concentration of Pb(Ⅱ) ($mg \cdot L^{-1}$), respectively; and C_a is the concentration of adsorbent ($g \cdot L^{-1}$).

2 Results and discussion

2.1 Characterization of the samples

The content of Ni in the as-prepared $Ni_{0.1}Fe_{2.9}O_4$, $Ni_{0.3}Fe_{2.7}O_4$ and $Ni_{0.6}Fe_{2.4}O_4$ is 2.1%, 6.8% and 13.7% (*w*/*w*), respectively. This indicates that the Ni is indeed incorporated into the Fe_3O_4 and the content of Ni in the $Ni_xFe_{3-x}O_4$(x=0.1, 0.3, and 0.6) increases with increasing the initial molar ratios of Ni/Fe. Fig.1 shows the powder XRD patterns of Fe_3O_4 and $Ni_xFe_{3-x}O_4$ (x=0.1, 0.3, and 0.6). The peaks of as-prepared Fe_3O_4 matches well with the file card of magnetite (PDF 89-0951). In the XRD patterns of $Ni_xFe_{3-x}O_4$, no extra peaks except the characteristic peaks of Fe_3O_4 could be detected. This shows that the doping of Ni^{2+} ions does not change the crystal structure of Fe_3O_4, and no second phase is introduced. However, there are some tiny changes in the intensity and width of the diffraction peaks. As the content of Ni increases, the peak intensity reduces slightly and

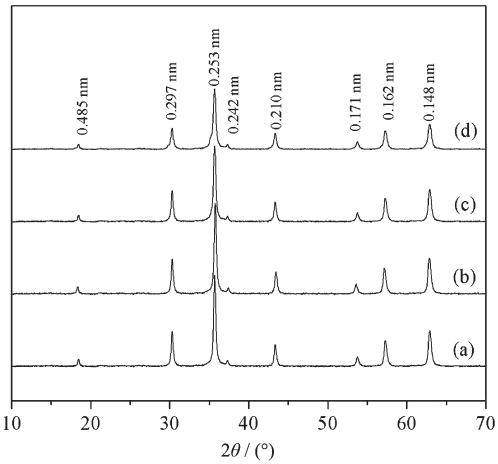

Fig.1 XRD patterns of (a) Fe_3O_4, (b) $Ni_{0.1}Fe_{2.9}O_4$, (c) $Ni_{0.3}Fe_{2.7}O_4$, and (d) $Ni_{0.6}Fe_{2.4}O_4$

the width at the peaks half height increases. This indicates that the as-prepared $Ni_xFe_{3-x}O_4$ possess a smaller particle size and a weaker crystallinity in comparison with Fe_3O_4.

SEM images of the samples are presented in Fig. 2. It can be seen that Fe_3O_4 and $Ni_xFe_{3-x}O_4$(x=0.1, 0.3, and 0.6) consist of approximately spherical shape particles of <50 nm. This indicates that the doping of Ni^{2+} ions does not significantly influence the micromorphology of Fe_3O_4. However, a higher content of Ni^{2+}

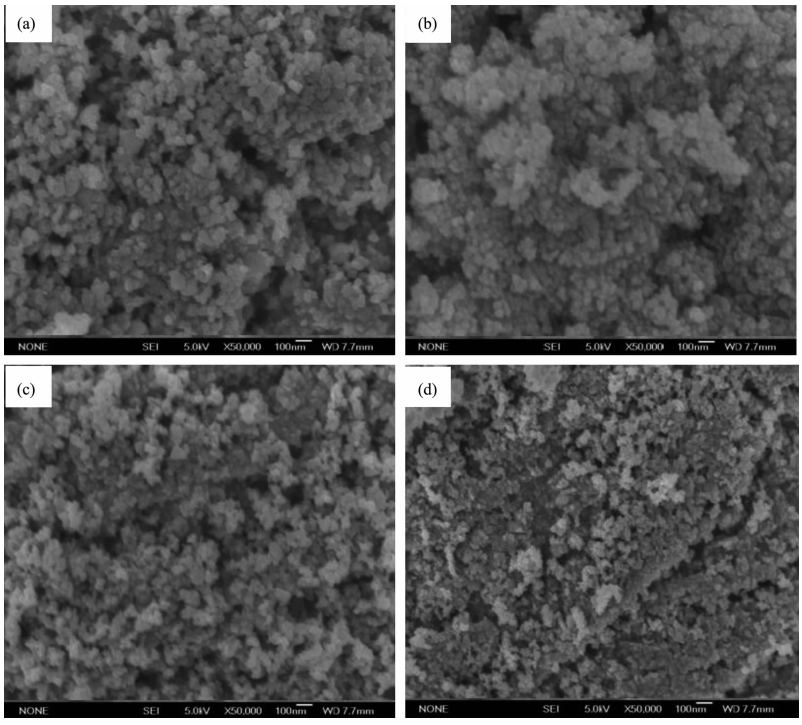

Fig.2 SEM micrographs of (a) Fe_3O_4, (b) $Ni_{0.1}Fe_{2.9}O_4$, (c) $Ni_{0.3}Fe_{2.7}O_4$, and (d) $Ni_{0.6}Fe_{2.4}O_4$

allows for a smaller particle size. The decrease in the particle size could be ascribed to the following factors: in the $Ni_xFe_{3-x}O_4$ structures, the higher crystal radius Fe^{2+} (0.074 nm) is replaced by the smaller ionic crystal radius Ni^{2+} (0.069 nm), and the crystallinity of $Ni_xFe_{3-x}O_4$ is relatively poorer than that of Fe_3O_4.

Fig.3 presents N_2-physisorption isotherms of the samples. All the adsorption isotherms are the type Ⅳ and the hysteresis loops are close to type H2. The hysteresis loop of this isotherm is associated with the filling and emptying of the mesopores by capillary condensation. Actually, there are no pores in the crystal structure of Fe_3O_4 [7]. Therefore, the mesopores of the samples should be the interparticle pores. The pore size distribution (PSD) curves of the samples are represented in the inset of Fig.3. All the samples show a broad and unsymmetrical peak, presenting the interparticle pores among the single particles and the microaggregates. In the PSD curves of Fe_3O_4, $Ni_{0.1}Fe_{2.9}O_4$, $Ni_{0.3}Fe_{2.7}O_4$ and $Ni_{0.6}Fe_{2.4}O_4$, the peaks corresponding to the main pore population appear at around 21.4, 20.7, 19.4 and 17.2 nm, respectively. This indicates that the main pore size decreases when the content of Ni increases, which is in agreement with the change trend of the particle size.

The total pore volumes, SSAs and surface fractal dimension D values of the samples increase in the sequence of $Fe_3O_4 < Ni_{0.1}Fe_{2.9}O_4 < Ni_{0.3}Fe_{2.7}O_4 < Ni_{0.6}Fe_{2.4}O_4$ (Table 1). This indicates that the doping of Ni^{2+} ions improves the porous structure of Fe_3O_4, and the pore structural heterogeneity and surface roughness of $Ni_xFe_{3-x}O_4$ are larger than those of Fe_3O_4.

Proton binding isotherms of the samples are shown in Fig.4 as a function of pH value at different KCl concentrations. The surface proton charge of the samples increases with increasing ionic strength. The pH value at the intersection point of the three q_H-pH curves is the pHpzc value of the sample, and they decrease with increasing the content of Ni.

At the background electrolyte of 20 mmol·L^{-1} KCl, some important data of potentiometric titrations are listed in Table 2. The total amount of H^+ ions

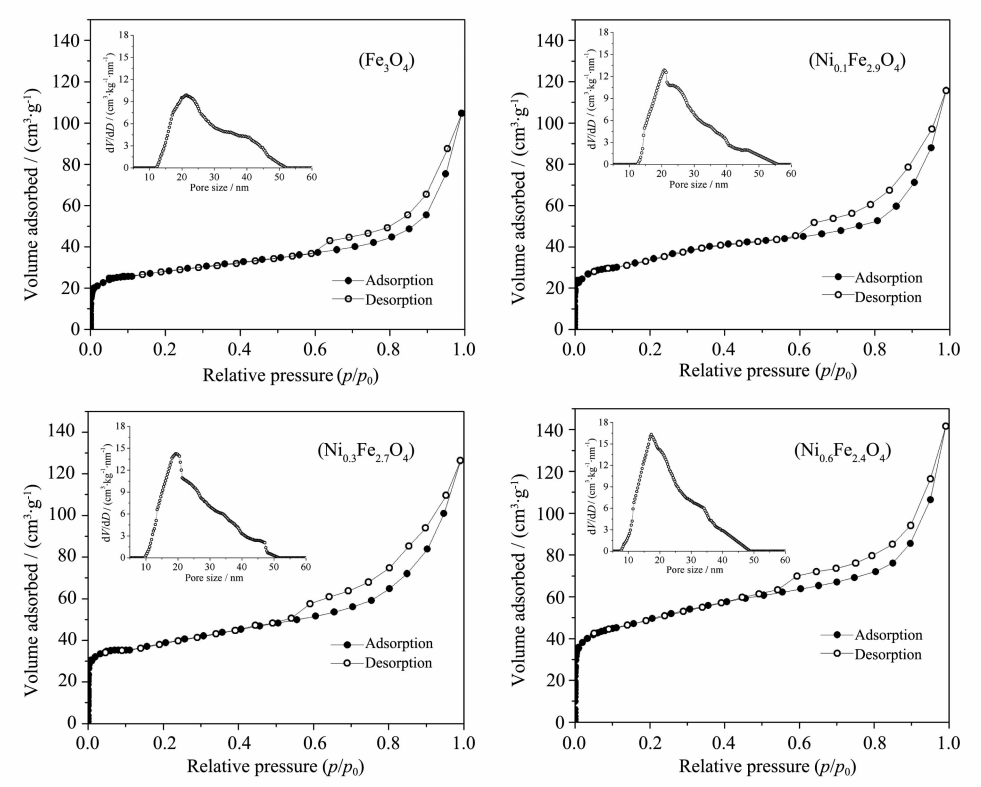

The corresponding pore size distributions from the desorption branch are showed in the inset

Fig.3　Nitrogen adsorption/adsorption isotherms of the samples

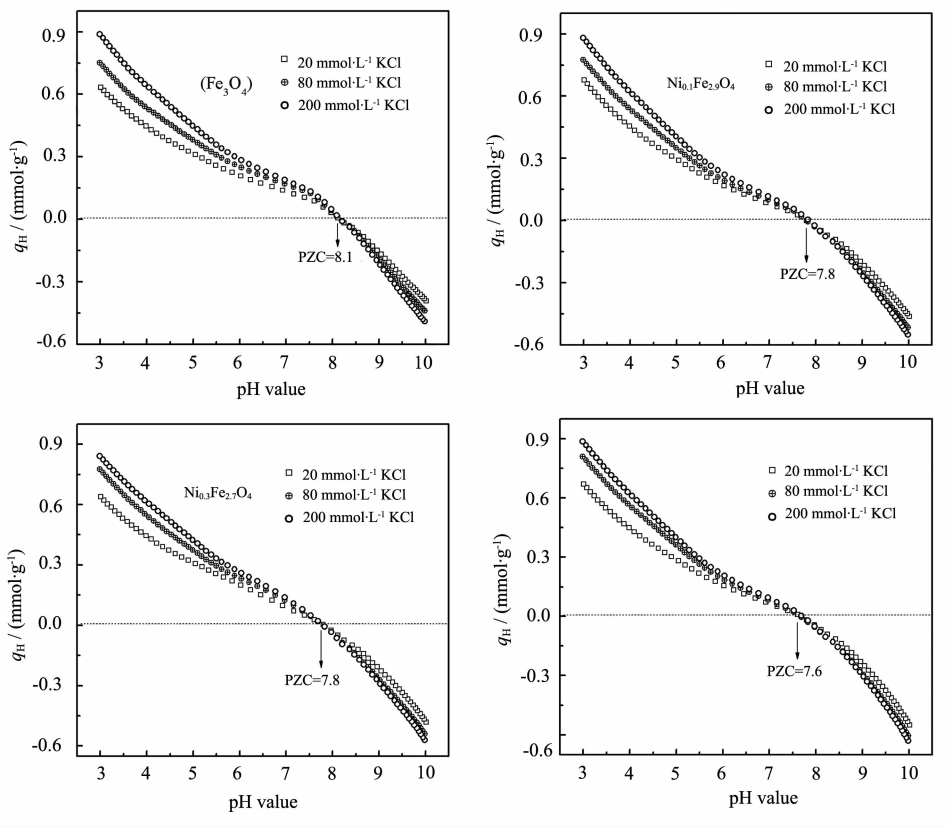

Fig.4 Proton binding isotherms as a function of pH value at different KCl concentrations

Table 1 Surface structural properties of the samples

Samples	Total pore volume / ($cm^3 \cdot g^{-1}$)	BET surface area / ($m^2 \cdot g^{-1}$)	Surface fractal dimension
Fe_3O_4	0.162	44	2.25
$Ni_{0.1}Fe_{2.9}O_4$	0.169	45	2.27
$Ni_{0.3}Fe_{2.7}O_4$	0.184	48	2.43
$Ni_{0.6}Fe_{2.4}O_4$	0.195	52	2.57

Table 2 Results of potentiometric titrations at the 20 mmol·L^{-1} KCl background electrolyte of the samples

Samples	Fe_3O_4	$Ni_{0.1}Fe_{2.9}O_4$	$Ni_{0.3}Fe_{2.7}O_4$	$Ni_{0.6}Fe_{2.4}O_4$
H^+ ions consumed from pH=10 to 3 / ($mmol \cdot g^{-1}$)	1.03	1.12	1.17	1.24
Surface proton charge at pH=5.0 / ($mmol \cdot g^{-1}$)	0.316	0.314	0.283	0.280

consumed from pH value of 10.0 to 3.0 is positively correlated to the surface hydroxyl content of the sample[17]. In the four samples, $Ni_{0.6}Fe_{2.4}O_4$ consumed the most H^+ ions when the pH value is adjusted from 10.0 to 3.0, indicating that $Ni_{0.6}Fe_{2.4}O_4$ nanoparticles possess the largest amounts of surface hydroxyls. This could be attributed to the fact that $Ni_{0.6}Fe_{2.4}O_4$ is in a poorly crystalline state. At pH value of 5.0, the surface positive charge of Fe_3O_4, $Ni_{0.1}Fe_{2.9}O_4$, $Ni_{0.3}Fe_{2.7}O_4$ and $Ni_{0.6}Fe_{2.4}O_4$ is 0.316, 0.314, 0.287 and 0.280 $mmol \cdot g^{-1}$, respectively. Clearly, at pH value of 5.0 the surface positive charge of the four samples decreases slightly with the increase in the content of Ni.

2.2 Pb(Ⅱ) adsorption by the samples

Fig.5 shows the equilibrium adsorption data for Pb (Ⅱ) on the samples. They are analyzed using Langmuir and Frieundlich models (Eqs. (**2**) and (**3**), respectively).

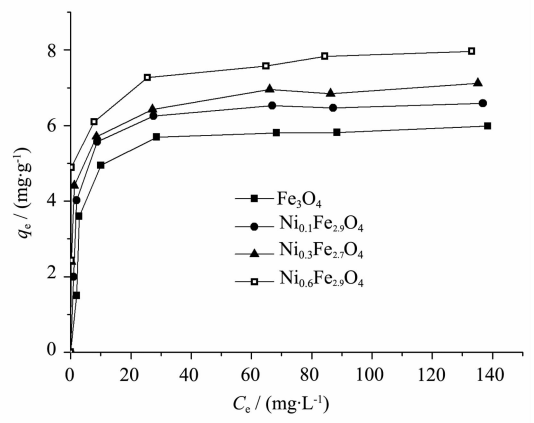

adsorbent dose: 2 g·L^{-1}; temperature: 25 ℃; background electrolyte: 20 mmol·L^{-1} KCl; contact time: 24 h; pH=5.0

Fig.5　Adsorption data for Pb(Ⅱ) by the samples

$$q_e = q_{max} bc_e/(1+bc_e) \quad (2)$$

$$q_e = kc_e^{1/n} \quad (3)$$

where q_e is the adsorption amount for Pb(Ⅱ) on adsorbent (mg·g^{-1}) and c_e is the residual concentration of Pb(Ⅱ) in the solution (mg·L^{-1})[18-19]; q_{max} and b in the Eq.(**2**) is the maximum adsorption capacity (mg·g^{-1}) and energy constant (L·mg^{-1}) of Langmuir model, respectively[18]; k (mg$^{1-1/n}$·L$^{1/n}$·g^{-1}) and $1/n$ (dimensionless) in the Eq.(**3**) is the Freundlich constant related to the adsorption capacity and adsorption intensity, respectively[19].

The results of fitting Langmuir and Frieundlich models to the adsorption data are summarized in Table 3. Both the Langmuir maximum adsorption capacity (q_{max}) and Freundlich adsorption capacity constants (k) of the samples show the order of Fe_3O_4< $Ni_{0.1}Fe_{2.9}O_4$ <$Ni_{0.3}Fe_{2.7}O_4$ <$Ni_{0.6}Fe_{2.4}O_4$. The Langmuir adsorption capacity for Pb(Ⅱ) increases from 6.02 mg·g^{-1} of Fe_3O_4 to 8.34 mg·g^{-1} of $Ni_{0.6}Fe_{2.4}O_4$. This can be understood by the following factors. Firstly, the total pore volume, SSA and surface fractal dimension of $Ni_{0.6}Fe_{2.4}O_4$ are larger than those of Fe_3O_4 (Table 1). According to literatures [6,17], the difference in the porosity properties contributes to the greater physical adsorption on $Ni_{0.6}Fe_{2.4}O_4$ than Fe_3O_4. Secondly, $Ni_{0.6}Fe_{2.4}O_4$ has a relatively lower pHpzc (7.6) and surface charge (0.280 mmol·g^{-1}) at pH value of 5.0 compared to Fe_3O_4. The decrease of the positive charge on the $Ni_{0.6}Fe_{2.4}O_4$ surface reduces the electrostatic repulsion between Pb(Ⅱ) ions and the surface of $Ni_{0.6}Fe_{2.4}O_4$. Thirdly, the reactive hydroxyl sites on $Ni_{0.6}Fe_{2.4}O_4$ are more than those of Fe_3O_4, which contributes to the Pb(Ⅱ) adsorption on $Ni_{0.6}Fe_{2.4}O_4$ through the surface coordination between Pb(Ⅱ) ions and the surface hydroxyls. Finally, the particle size of $Ni_{0.6}Fe_{2.4}O_4$ is smaller than that of Fe_3O_4, and probably a special nanoscale size-effect also contributes to a higher Pb(Ⅱ) adsorption on $Ni_{0.6}Fe_{2.4}O_4$.

The Langmuir correlation coefficients for Pb(Ⅱ) adsorption by the samples are fairly high (R^2=0.994 2 ~0.985 8) and they follow the order of Fe_3O_4 > $Ni_{0.1}Fe_{2.9}O_4$ >$Ni_{0.3}Fe_{2.7}O_4$ =$Ni_{0.6}Fe_{2.4}O_4$. The correlation coefficients of Freundlich model are relatively low (R^2=0.981 3~0.947 7) and they increase in the order of Fe_3O_4<$Ni_{0.1}Fe_{2.9}O_4$<$Ni_{0.3}Fe_{2.7}O_4$<$Ni_{0.6}Fe_{2.4}O_4$. This can be explained by the following factors. As for Fe_3O_4, the ≡Fe-OH groups are the main reactive sites for Pb(Ⅱ) adsorption [5-6], and the surface fractal dimension D value (2.25) is lower. This indicates that Fe_3O_4 possesses a homogeneous surface with identical adsorption sites. Therefore, the Pb(Ⅱ) adsorption data by Fe_3O_4 are well fitted by Langmuir model. For $Ni_{0.6}Fe_{2.4}O_4$, the surface reactive sites include ≡Fe-OH and ≡Ni-OH groups, and the D value (2.57) is relatively high. This indicates that the doping of Ni^{2+}

Table 3　Parameters of fitting Langmuir and Freundlich models to the adsorption data for Pb(Ⅱ) by the samples

Samples	Langmuir model			Freundlich model		
	q_{max} / (mg·g^{-1})	b	R^2	k	n	R^2
Fe_3O_4	6.02	4.72	0.994 2	5.46	0.283	0.947 7
$Ni_{0.1}Fe_{2.9}O_4$	6.68	4.55	0.990 8	5.08	0.261	0.950 2
$Ni_{0.3}Fe_{2.7}O_4$	7.29	4.17	0.986 4	4.74	0.227	0.967 3
$Ni_{0.6}Fe_{2.4}O_4$	8.34	3.61	0.985 8	4.27	0.175	0.981 3

into Fe_3O_4 increases the surface heterogeneity of the products. Therefore, the Freundlich correlation coefficients of $Ni_xFe_{3-x}O_4$ are higher than that of Fe_3O_4.

For the Pb (Ⅱ) adsorption data of Fe_3O_4, the correlation coefficient of Langmuir is significantly higher than that of Freundlich. This indicates that mono-layer adsorption model is important in adsorbing Pb (Ⅱ) onto the Fe_3O_4 surface. Therefore, the Pb (Ⅱ) adsorption capacity of Fe_3O_4 is relatively low. For the Pb (Ⅱ) adsorption data of $Ni_{0.6}Fe_{2.4}O_4$, the correlation coefficient of Freundlich is close to that of Langmuir, indicating that multilayer adsorption model is also important for the Pb (Ⅱ) adsorption on $Ni_{0.6}Fe_{2.4}O_4$. Therefore, the Pb(Ⅱ) adsorption capacity of $Ni_{0.6}Fe_{2.4}O_4$ is much higher than that of Fe_3O_4. The present results lead to a better understanding of the Pb(Ⅱ) adsorption by Ni-doped magnetites, and also show that the Ni-doped magnetite, $Ni_{0.6}Fe_{2.4}O_4$-like, is a better adsorbent for Pb (Ⅱ) removal from aqueous solutions compared to Fe_3O_4.

3 Conclusions

Ni-doped magnetites ($Ni_xFe_{3-x}O_4$, x=0.1, 0.3, and 0.6) nanoparticles were prepared by a modified coprecipitation procedure. The surface properties and Pb (Ⅱ) adsorption capacities of $Ni_xFe_{3-x}O_4$ are significantly influenced due to the doping of Ni^{2+} ions into Fe_3O_4, and the magnitude of the effect increases consistently with the increase in the content of Ni. Compared to Fe_3O_4, the crystal structure and micromorphologies of $Ni_xFe_{3-x}O_4$ nanoparticles remain nearly unchanged; the particle size of $Ni_xFe_{3-x}O_4$ becomes smaller; the porous structures are greatly improved; and the pHpzc value and the positive surface charge at pH value of 5.0 are decreased. Langmuir correlation coefficients for Pb(Ⅱ) adsorption by the samples are higher and they follow the order of Fe_3O_4 >$Ni_{0.1}Fe_{2.9}O_4$ >$Ni_{0.3}Fe_{2.7}O_4$ =$Ni_{0.6}Fe_{2.4}O_4$. The correlation coefficients of Freundlich model are lower, and they increase consistently with increasing the content of Ni. The Langmuir adsorption capacities (q_{max}) and Freundlich adsorption capacity constants (k) for Pb(Ⅱ) ions by $Ni_xFe_{3-x}O_4$ are higher than those of Fe_3O_4. Results in present study show that $Ni_xFe_{3-x}O_4$ and $Ni_{0.6}Fe_{2.4}O_4$-like are better adsorbents for the removal of Pb(Ⅱ) from aqueous solutions compared to Fe_3O_4, and probably monolayer and multilayer adsorption behaviors are simultaneously involved in the Pb(Ⅱ) adsorption on $Ni_xFe_{3-x}O_4$.

References:

[1] Li R J, Chang X J, Li Z H, et al. *Microchim. Acta*, **2011**, **172**:269-276

[2] Ponder S M, Darab J G, Mallouk T E. *Environ. Sci. Technol.*, **2000**,**34**:2564-2569

[3] Tran H V, Tran L D, Nguyen T N. *Mater. Sci. Eng. C*, **2010**, **30**:304-310

[4] Imamoglu M, Tekir O. *Desalination*, **2008**,**228**:108-113

[5] Chang Y C, Chen D H. *J. Colloid Interf. Sci.*, **2005**,**283**: 446-451

[6] Liu J F, Zhao Z S, Jiang G B. *Environ. Sci. Technol.*, **2008**, **42**:6949-6954

[7] Illés E, Tombácz E. *Colloids Surf. A*, **2003**,**230**:99-109

[8] Sidhu P S, Gilkes R J, Posner A M. *J. Inorg. Nucl. Chem.*, **1978**,**40**:429-435

[9] Liang X, Zhong Y, Tan W, et al. *J. Therm. Anal. Calorim.*, **2013**,**111**:1317-1324

[10]Mohapatra J, Mitra A, Bahadur D, et al. *Cryst. Eng. Comm.*, **2013**,**15**:524-532

[11]Mathur B S, Venkataramani B. *Colloids Surf. A*, **1998**,**140**: 403-416

[12]Lelis M F, Rios R V, Lago R M, et al. *Hyperfine Interact.*, **2002**(C):345-349

[13]Chun C L, Baer D R, Matson D W, et al. *Environ. Sci. Technol.*, **2010**,**44**:5079-5085

[14]Singh N K, Singh R N. *Indian J. Chem. A*, **1999**,**38**:491-495

[15]Lelis M D F F, Fabris J D, Mussel W D N, et al. *Mater. Res.*, **2003**,**6**:145-150

[16]Kittaka S, Morimoto T. *J. Colloid Interf. Sci.*, **1980**,**75**:398-403

[17]Tombácz E, Libor Z, Illés E. *Org. Geochem.*, **2004**,**35**:257-267

[18]Langmuir I. *J. Am. Chem. Soc.*, **1916**,**40**:1361-1368

[19]Freundlich H M F. *J. Phys. Chem. B*, **1906**,**57**:385-470